Robust Electrocatalysts from Metal Doped $W_{18}O_{49}$ Nanofibers for High-Efficiency Hydrogen Evolution

Yuanyuan Zhao, Qunwei Tang[*], Peizhi Yang, and Benlin He

*Email address: tangqunwei@ouc.edu.cn; Tel: (86) 532-66782533.

Experimental Section

Materials: WCl_5 and $PdCl_2$ were purchased from Aladdin. Pt/C (20 wt% Pt) was purchased from Johnson Matthey. Nafion solution (5 wt%) was purchased from Sigma-Aldrich. All chemicals were used as received without any further purification.

Synthesis of $W_{18}O_{49}$ Nanostructures: $W_{18}O_{49}$ NFs, NFBs and MSs were prepared by dissolving 0.1, 0.17 and 0.5 g of WCl_6 in 50 mL ethanol, which was then transferred into a Teflon-lined autoclave. After being heated at 180℃ for 24 h, the mixture was cooled to room temperature naturally. The product was subsequently collected by centrifugation and washed repeatedly with water and ethanol. Finally, the samples were dried under vacuum at 45 ℃ overnight. Pd doped $W_{18}O_{49}$ NFs were synthesized by the same facile and template-free solvothermal method. In details, the solution was prepared by dissolving 0.1g WCl_6 and stoichiometric $PdCl_2$ (0.22 mg for 1 at% Pd doped $W_{18}O_{49}$ NFs, 1.12 mg for 5 at% Pd doped $W_{18}O_{49}$ NFs, and 2.24 mg for 10 at% Pd doped $W_{18}O_{49}$ NFs) in 50 mL ethanol. The subsequent procedures are identical to the aforementioned preparation process of $W_{18}O_{49}$ NFs, NFBs and MSs.

Fabrication of Electrodes: Catalyst ink was prepared by dispersing 5 mg of catalyst into 990 μL of isopropanol containing 10 μL of 5 wt% Nafion, which was then sonicated for 30 min. Finally, 5 of the catalyst ink was loaded onto a glassy carbon electrode (GCE) of 3 mm in diameter. The

electrocatalyst loading amount was controlled at 0.35 mg cm^{-2} for each catalytic electrode.

Electrochemical Characterizations: All electrochemical measurements were conducted on a CHI660E electrochemical workstation in a typical three-electrode setup, which comprising an Ag/AgCl reference electrode, a counter electrode (CE) composed of a Pt sheet, and a working electrode of GCE supported catalyst. The polarization curves were recorded with a linear sweep voltammetry (LSV) mode and at a scan rate of 1 mV s^{-1} in 0.5 M H$_2$SO$_4$ aqueous solution. Tafel plots were also obtained under the same conditions. Onset overpotentials were determined according to the beginning of the linear regime in the Tafel plots. Electrochemical impedance spectroscopy (EIS) measurements were conducted in the frequency range of 10^6 Hz ~ 10^{-2} Hz. The long-term stability was tested at η = 503 mV in 0.5 M H$_2$SO$_4$ aqueous solution. In all measurements, the Ag/AgCl reference electrode was calibrated with respect to reversible hydrogen electrode (RHE). In 0.5 M H$_2$SO$_4$, E$_{RHE}$=E$_{Ag/AgCl}$+0.197V. Due to the effects from ohmic resistance, the as-measured currents cannot demonstrate the intrinsic charge-transfer behaviors of catalytic electrodes. To address this issue, an iR compensation has been applied to all electrochemical characterizations. When the UV/Vis/NIR absorption spectra was tested, the concentrations of all target solutions were controlled at 0.01 mg/mL

Other Characterizations: The scanning electron microscopy (SEM) images were obtained on SU8010 and S4800. Transmission electron microscopy (TEM) images were obtained on Tecnai G2 F20 FEI instruments. X-ray diffraction (XRD) data were obtained on BRUCKER D8 Advance with Cu Kα radiation (λ=1.5418 Å). The BET surface area, pore volume, and pore size were measured on a ASAP 2020 at liquid N$_2$ temperature. X-ray Photoelectron Spectroscopy (XPS) spectra were recorded with a Thermo Scientific Escalab 250 Xi.

Supporting Tables and Figures

Table S1. Structural parameters of pristine $W_{18}O_{49}$ NFs, 1, 5 and 10 at% Pd doped $W_{18}O_{49}$ NFs obtained from XRD patterns.

Electrode materials	β (°)	2θ (°)	Crystallite size (nm)	$\Delta d/d$
Pristine $W_{18}O_{49}$ NFs	0.45	23.47	17.84	0.009
1 at% Pd doped $W_{18}O_{49}$ NFs	0.53	23.46	15.15	0.011
5 at% Pd doped $W_{18}O_{49}$ NFs	0.59	23.43	13.61	0.012
10 at% Pd doped $W_{18}O_{49}$ NFs	0.55	23.45	14.60	0.011

Table S2. A comparison of HER performances for various electrode materials in acid media. Onset η refers to onset overpotential; j is the current density , η is the corresponding overpotential at j, b is the Tafel slope and j_0 is the exchange current density.

Electrode materials	Onset η /mV	j/mA cm^{-2}	η at the corresponding j/mV	b/mV dec^{-1}	j_0/mA cm^{-2}	Ref.
$W_{18}O_{49}$ MSs	227	10	552	-	-	
		50	656			
		100	789			
$W_{18}O_{49}$ NFBs	119	10	530	-	-	
		50	643			
		100	754			
$W_{18}O_{49}$ NFs	110	10	425	54	1.90×10^{-3}	
		50	587			
		100	678			This work
1 at% Pd doped $W_{18}O_{49}$ NFs	93	10	331	-	-	
		50	481			
		100	605			
5 at% Pd doped $W_{18}O_{49}$ NFs	65	10	137	35	2.36×10^{-3}	
		50	288			
		100	406			
10 at% Pd doped $W_{18}O_{49}$ NFs	72	10	164	-	-	
		50	361			
		100	522			
MoP-CA2 (Mo:P:citric acid=1:1:2)	40	2	84	54	0.086	1

		10	125			
		100	200			
WS_2 nanoflakes	100	-	-	48	-	2
nitrogen-enriched carbon-encapsulated cobalt nanoparticles dispersed on graphene sheets	70	10	265	98	-	3
double-gyroid MoS_2/fluorine-doped tin oxide	150-200	2	190	50	6.9×10^{-4}	4
defect-rich MoS_2	120	13	200	50	8.9×10^{-3}	5
$NiMoN_x$/C	78	5	220	35.9	0.24	6
Core-shell MoO_3-MoS_2 nanowires on fluorine-doped tin oxide	150-200	10	310	50-60	8.2×10^{-5}	7
cobalt-embedded nitrogen-rich carbon nanotubes	50	1 10	140 260	69	0.01	8
FeP nanosheets	100	10	～240	67	-	9
Mixed Close-Packed Cobalt Molybdenum Nitrides ($Co_{0.6}Mo_{1.4}N_2$)	-	10	200		0.23	10
monolayer Pt/Au nanofilm/Ni foam	40	70	400	53	-	11
Co_2P/Ti	-	10 20	95 109	45	-	12
MoS_2/tetracyanoquinodimethane/carbon cloth	-	51 209	200 300	40	-	13
self-supported nanoporous cobalt phosphide nanowire arrays on carbon cloth	38	10 20 100	67 100 204	c51	0.288	14

|						
MoS$_3$ particles	100	2	190	54	6.3×10^{-4}	15
WS$_2$/Reduced Graphene Oxide	150-200	23	300	58	-	16
CoSe$_2$ nanobelts	50	-	-	48	8.4×10^{-3}	17
Carbon-supported molybdenum nitride nanosheets	157	2	290	54.5	3.6×10^{-2}	18
molybdenum sulfide films deposited on fluorine-doped tin oxide	120	2	170	40	1.3×10^{-4}	19

Table S3. The low-frequency R_{ct} and electron lifetime (τ) for 5 at% Pd doped $W_{18}O_{49}$ NFs electrode at various HER overpotentials.

| Overpotentials (mV)	65	100	150	200	300
R_{ct} (ohm cm^2)	66.5	28.8	10.6	4.4	1.2
f	0.0825	0.1	0.215	0.562	1.78
τ (s)	1.93	1.59	0.74	0.28	0.09
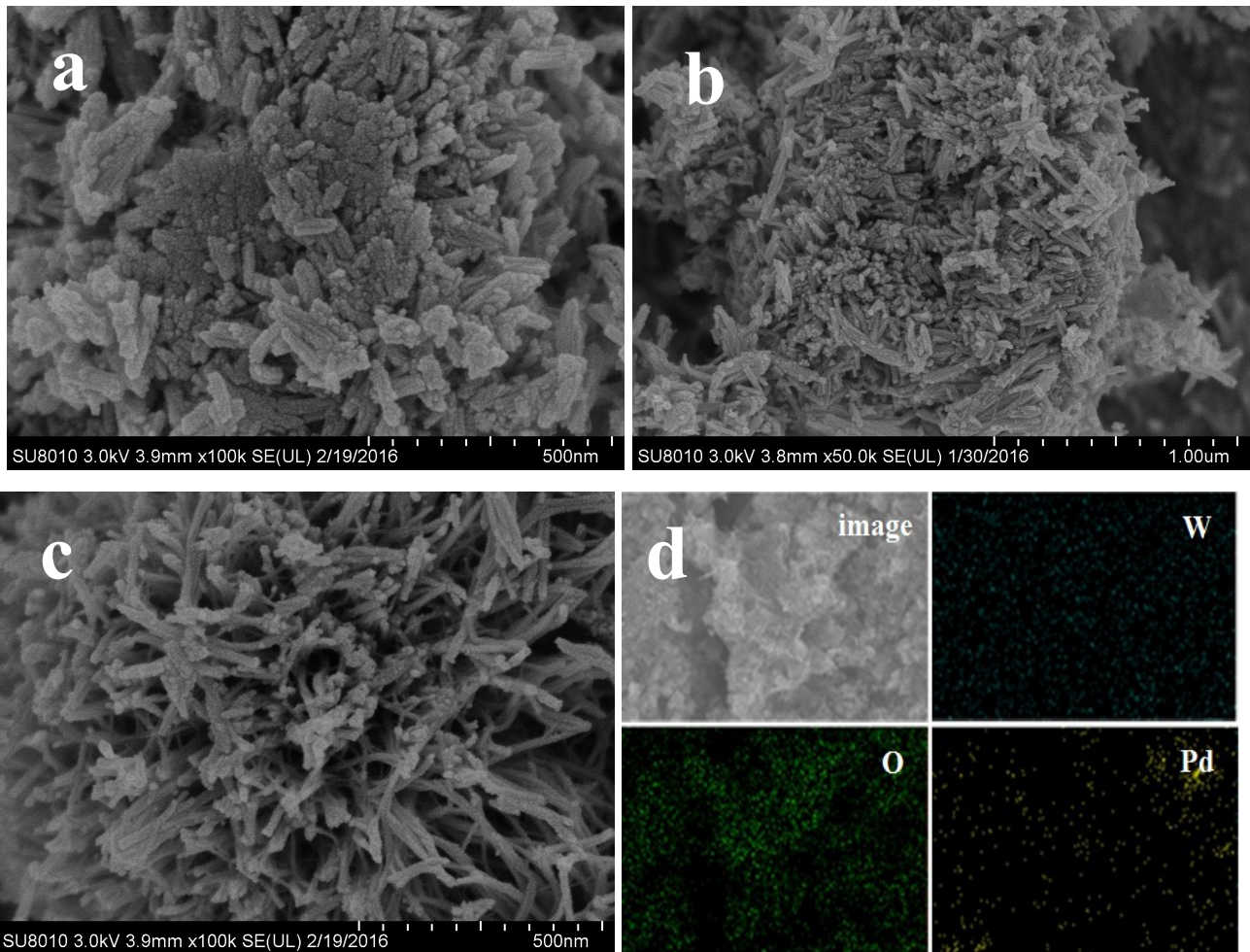
Figure S1. SEM images of (a) 1 at% Pd doped $W_{18}O_{49}$ NFs, (b) 5 at% Pd doped $W_{18}O_{49}$ NFs and (c) 10 at% Pd doped $W_{18}O_{49}$ NFs. (d) Elemental mapping images of W, O, and Pd for 5 at% Pd doped $W_{18}O_{49}$ NFs.
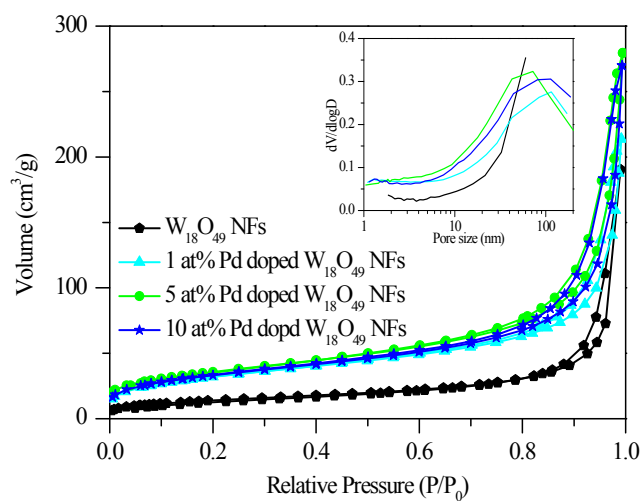
Figure S2. Nitrogen adsorption/desorption isotherm plots for pristine $W_{18}O_{49}$ NFs and Pd doped $W_{18}O_{49}$ NFs.

Figure 1d shows a closely packed 5 at% Pd doped $W_{18}O_{49}$ NFs having heterogeneous diameters with gigantic aspect ratio. 1 at% Pd doped $W_{18}O_{49}$ NFs (Figure S1a) tend to aggregate together while 10 at% Pd doped $W_{18}O_{49}$ NFs tend to bundle together automatically (Figure S1b). BET characterization yields increased specific surface area of 113.9, 126.3 and 118.2 m^2 g^{-1} for 1, 5 and 10 at% Pd doped $W_{18}O_{49}$ NFs (Figure S2). Regardless of other performances, increased specific surface area for an electrocatalyst is expected to provide enhanced catalytic activity.
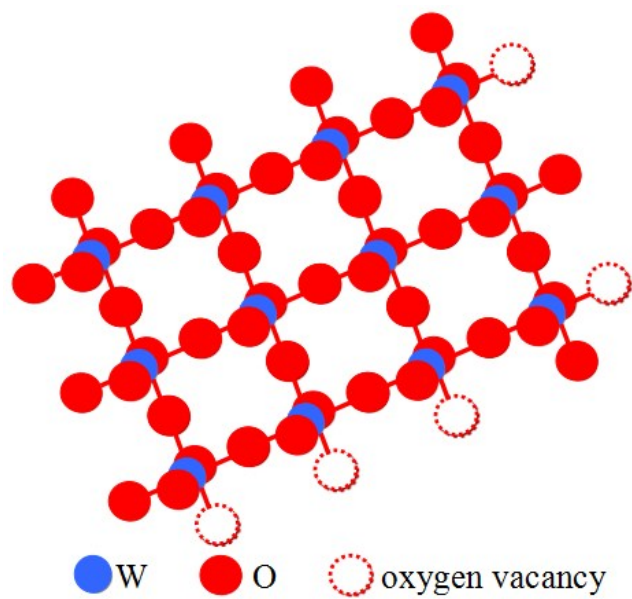
Figure S3. Schematic illustrating for pristine $W_{18}O_{49}$ structure.
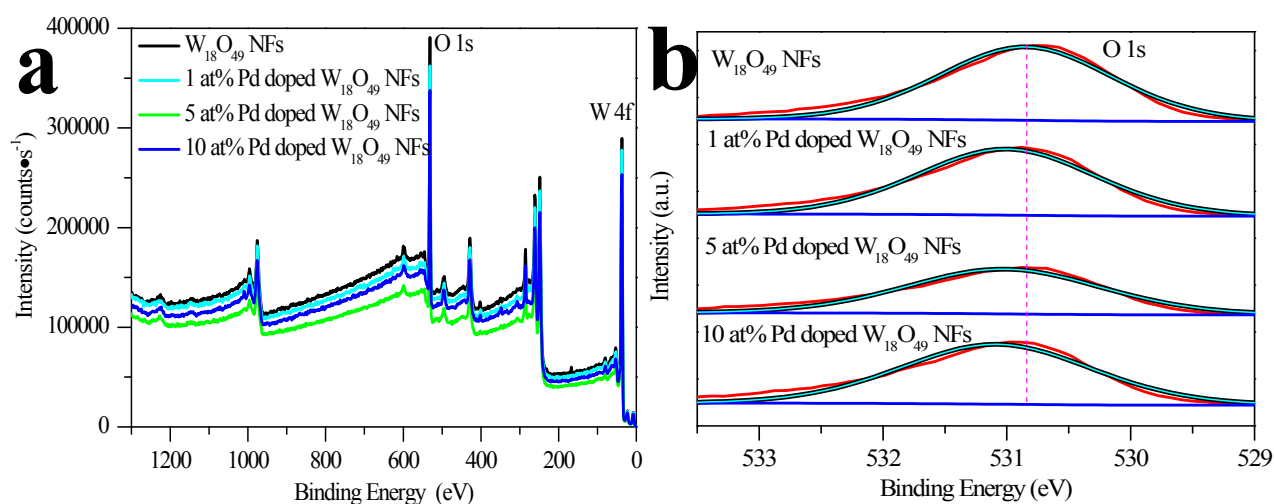
Figure S4. XPS spectrum: (a) survey spectrum, (b) O 1s peaks for pristine $W_{18}O_{49}$ NFs and Pd doped $W_{18}O_{49}$ NFs.

XPS characterizations for the chemical valence of W species yield a doublet peak for W4f$_{5/2}$ and W4f$_{7/2}$. The percentages of W^{5+} states for 1, 5 and 10 at% Pd doped $W_{18}O_{49}$ NFs are 60.76%, 63.75% and 61.58%, respectively. The O 1s peak of pure W18O49 NFs shows a single Gaussian component centered at 530.78 eV, and the value is close to the commonly reported value of 530.6 eV (Figure 2d). The binding energies were shifted to higher values after the addition of Pd.
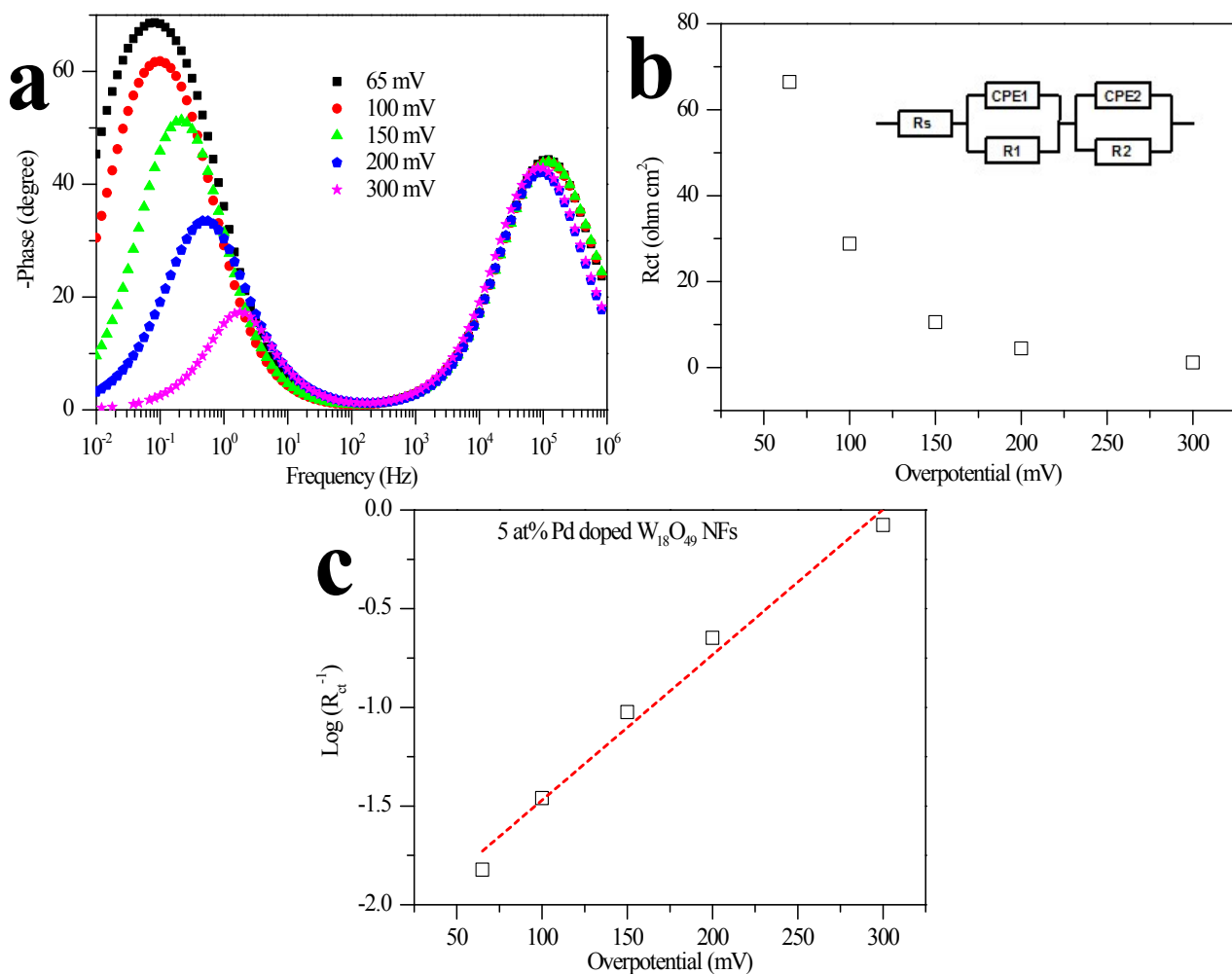
Figure S5. (a) Bode EIS plots，(b) The low-frequency charge-transfer resistance (R_{ct}) and equivalent electrical circuit used to model the HER process and plots of log (R_{ct}^{-1}) as a function of overpotential for 5 at% Pd doped $W_{18}O_{49}$ NFs recorded in 0.5 M H_2SO_4 aqueous solution.

Supporting References

[1] Z. C. Xing, Q. Liu, A. M. Asiri and X. P. Sun, *Adv. Mater.*, 2014, **26**, 5702-5707.

[2] L. Cheng, W. J. Huang, Q. F. Gong, C. H. Liu, Z. Liu, Y. G. Li and H. J. Dai, *Angew. Chem. Int. Ed.*, 2014, **53**, 7860 -7863.

[3] H. L. Fei, Y. Yang, Z. W. Peng, G. D. Ruan, Q. F. Zhong, L. Li, E. L. G. Samuel and J. M. Tour, *ACS Appl. Mater. Interfaces*, 2015, **7**, 8083-8087.

[4] J. Kibsgaard, Z. Chen, B. N. Reinecke and T. F. Jaramillo, *Nat. Mater.*, 2012, **11**, 963-969.

[5] J. Xie, H. Zhang, S. Li, R. Wang, X. Sun, M. Zhou, J. Zhou, X. Lou and Y. Xie, *Adv. Mater.*, 2013, **25**, 5807-5813.

[6] W. F. Chen, K. Sasaki, C. Ma, A. I. Frenkel, N. Marinkovic, J. T. Muckerman, Y. M. Zhu and R. R. Adzic, *Angew. Chem. Int. Ed.*, 2012, **51**, 6131-6135.

[7] Z. Chen, D. Cummins, B. N. Reinecke, E. Clark, M. K. Sunkara and T. F. Jaramillo, *Nano Lett.*, 2011, **11**, 4168-4175.

[8] X. Zhu, X. Huang, A. Goswami, R. Silva, B. R. Sathe, E. Mikmekova and T. Asefa, *Angew. Chem. Int. Ed.*, 2014, **53**, 4372-4376.

[9] Y. Xu, R. Wu, J. Zhang, Y. Shi and B. Zhang, *Chem. Commun.*, 2013, **49**, 6656-6658.

[10] B. Cao, G. M. Veith, J. C. Neuefeind, R. R. Adzic and P. G. Khalifah, *J. Am. Chem. Soc.*, 2013, **135**, 19186-19192.

[11] M. Li, Q. Ma, W. Zi, X. J. Liu, X. J. Zhu and S. Z. Liu, *Science Advances*, 2015, **4**, DOI: 10.1126/sciadv.1400268.

[12] J. F. Callejas, C. G. Read, E. J. Popczun, J. M. McEnaney and R. E. Schaak, *Chem. Mater.*, 2015, **27**, 3769-3774.

[13] Y. H. Chang, R. D. Nikam, C. T. Lin, J. K. Huang, C. C. Tseng, C. L. Hsu, C. C. Cheng, C. Y. Su, L. J. Li and D. H.C. Chua, *ACS Appl. Mater. Interfaces*, 2014, **6**, 17679-17685.

[14] J. Q. Tian, Q. Liu, A. M. Asiri and X. P. Sun, *J. Am. Chem. Soc.*, 2014, **136**, 7587-7590.

[15] H. Vrubel，D. Merki and X Hu, *Energy Environ. Sci.*, 2012, **5**, 6136-6144.

[16] J. Yang, D. Voiry, S. J. Ahn, D. Kang, A. Y. Kim, M. Chhowalla and H. S. Shin, *Angew. Chem. Int. Ed.*, 2013, **52**, 13751-13754.

[17] Y. F. Xu, M. R. Gao, Y. R. Zheng, J. Jiang and S. H. Yu, *Angew. Chem. Int. Ed.*, 2013, **52**, 8546-8550.

[18] W. F. Chen, K. Sasaki, C. Ma, A. I. Frenkel, N. Marinkovic,J. T. Muckerman, Y. Zhu and R. R. Adzic, *Angew. Chem. Int. Ed.*, 2012, **51**, 6131-6135.

[19] D. Merki, S. Fierro, H. Vrubel and X. Hu, *Chem. Sci.*, 2011, **2**, 1262-1267.